Development of a computational tool for the aerodynamic simulation of a wing-flap

Jorge André Fernandes Baginha
jorgebaginha@ist.utl.pt

Instituto Superior Técnico, Lisboa, Portugal

October 2013

Abstract

The main purpose of the present work was to develop a computational tool used to predict the aeorodynamic characteristics of a wing-flap. The 3D panels method using the Dirichlet-type boundary condition was adopted to obtain the inviscid flow. The latter allowed the consideration of the ground effect through the use of the images method. In order to consider the viscid effects, the geometry was discretized/divided into bidimensional cross sections. Each of them was individualy analysed by XFOIL program/routine. The coupling of both solutions was done by means of a transpiration velocity. The inviscid and viscous flows solutions were compared with experimental data obtained for two different types of wings and for a wing-flap aggregate. The results were satisfactory in the sense that the relative erros between the computational and experimental data were small. We concluded that the developed code may constitute, as a first approach, a valuable computational tool to be used in the design of rigid sails

Keywords: 3D Panel Method, Dirichlet Boundary Condition, Ground Effect, Viscous Effects

1 Introduction

The main purpose of this study is the construction of a computational tool able to predict the aerodynamic characteristics of a sustaining surface. The final end of this tool is its inclusion on the rigid sails project (wing sails) of catamarans dedicated to high competition. In fact, this work follows on a partnership developed between the Optimal Structural Solution [1] and Tony Castro [2] for the construction to the first fully portuguese catamaran participating in the International C-Class Catamaran Competition (ICCCC). To this end, Optimal Structural Solutions suggested to the Instituto Superior Técnico, the elaboration, by students of the master's degree in aerospace engineering, of a thesis with a theme "Development of simulation tool for catamaran solid sails".

The ICCCC is a competition where each participating team develops its own catamaran, and, although there are some restrictions catamaran geometrical length, width, and area of the sail, there is given great degree of freedom in what concern to its design in its construction, in this way, thus promoting the search for the most advanced technologies especially in aerodynamic and hydrodynamic field and materials. In this kind of wing sail, which emerged in the 80's, the wing is thick contrary to what happens in conventional sails. The rigid wing sails are formed by two surfaces: the main element and the flap, which serves to add camber on the wing sail, increasing the resulted force.

Given the circumstances of the sail operation, it was considered appropriate to include in the computational tool the influence of water surface as well as the variation of velocity within the atmospheric boundary layer.

It is in this context that this work will be developed.

2 Panel Method 3D

2.1 The Mathematical Modeling of the Problem

Consider a body with known boundaries S_B, submerged in a potential flow, as shown in Fig. 1, the external flow (V region) is incompressible, irrotational and inviscid. The potential velocity can be obtained by solving the Laplace equation:

$$\nabla^2 \Phi^* = 0 \tag{1}$$

The solution of Eq. 1 can be constructed, according Green [3, 4], by the sum of source σ and doublet μ distributions placed on the boundary surface S_B:

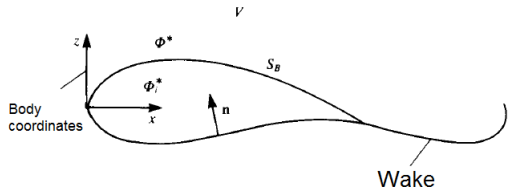

Figure 1: Potential flow over a close body. [3]

$$\Phi^*(x,y,z) = -\frac{1}{4\pi}\int_{S_B}\left[\sigma\left(\frac{1}{r}\right) - \mu\mathbf{n}\cdot\nabla\left(\frac{1}{r}\right)\right]dS + \tag{2}$$
$$+\,\Phi_\infty$$

where $\mathbf{n}$ is the normal vector pointing to inside the body, r the distance between the field point P and the element dS and Φ_∞ is the free-stream potential.

2.2 Dirichlet Boundary Condition

In the Dirichlet problem, the zero normal velocity on the surface $\nabla(\Phi_i^*)\cdot\mathbf{n} = 0$ results $\Phi_i^* = (\Phi+\Phi_\infty)_i = const$. So, for a close body, the inner velocity potential don't change,

$$\Phi_i^*(x,y,z) = \frac{1}{4\pi}\int_{corpo+esteira}\mu\frac{\partial}{\partial n}\left(\frac{1}{r}\right)dS - \tag{3}$$
$$-\frac{1}{4\pi}\int_{corpo}\sigma\left(\frac{1}{r}\right)dS + \Phi_\infty = const$$

The Eq. 3 is the basis for the the methods that use Dirichlet boundary condition.

In this work the inner velocity potential is selected to be equal to Φ_∞:

$$\frac{1}{4\pi}\int_{corpo+esteira}\mu\frac{\partial}{\partial n}\left(\frac{1}{r}\right)dS - \tag{4}$$
$$-\frac{1}{4\pi}\int_{corpo}\sigma\left(\frac{1}{r}\right)dS = 0 \tag{5}$$

and for this case the source strengh can be written as:

$$\sigma = \mathbf{n}\cdot\mathbf{Q}_\infty \tag{6}$$

2.3 Numerical Implementation

The body is divided into N flat panels and the wake into N_w. The boundary condition will be specified at the central point of each flat panel, named control points.

The Eq. 4 for each control point:

$$\sum_{k=1}^{N}\frac{1}{4\pi}\int_{Painel-corpo}\mu\mathbf{n}\cdot\nabla\left(\frac{1}{r}\right)dS -$$
$$-\sum_{k=1}^{N}\frac{1}{4\pi}\int_{Painel-corpo}\sigma\left(\frac{1}{r}\right)dS +$$
$$+\sum_{l=1}^{N_w}\frac{1}{4\pi}\int_{Painel-esteira}\mu\mathbf{n}\cdot\nabla\left(\frac{1}{r}\right)dS = 0. \tag{7}$$

Note that the integration in Eq. 7, unlike Eq. 4, is limited to each individual panel element. In case of doublet and source distribution on each panel the influence of panel k at point P is,

$$C_k = \frac{1}{4\pi}\int_{Painel-corpo}\frac{\partial}{\partial n}\left(\frac{1}{r}\right)dS, \tag{8}$$

$$B_k = -\frac{1}{4\pi}\int_{Painel-corpo}\left(\frac{1}{r}\right)dS. \tag{9}$$

The Equations 8 and 9 represent the influence coeficient for dipole and source, respectively. This coefficients can be calculated using Eq. 32 and 33 for flat panels and constant strength singularity.

The Eq. 7 can be reduced to:

$$\sum_{k=1}^{N}C_k\mu_k + \sum_{k=1}^{N}B_k\sigma_k + \sum_{l=1}^{N_w}C_l\mu_l = 0. \tag{10}$$

This is the numerical expression for an aplication of boundary condition.

The strength of source panel σ_k can be calculated by Eq. 6 where $\mathbf{n}$, now, is the normal vector to the panel k,

$$\sigma_k = \mathbf{n_k}\cdot\mathbf{Q}_\infty, \tag{11}$$

The strength of wake doublet panels μ_l can be related with the strength of trailing edge panels by Kutta condition (Fig. 2),

$$\mu_t = \mu_r - \mu_s. \tag{12}$$

For example, the application of boundary condition equation, 10, on control point number 1 result in the expression:

$$C_{11}\mu_1 + \ldots + (C_{1r}+C_{1t})\mu_r + \tag{13}$$
$$+\,(C_{1s}-C_{1t})\mu_s + \ldots \tag{14}$$
$$\ldots + C_{1N}\mu_N + \sum_{k=1}^{N}B_k\sigma_k = 0$$

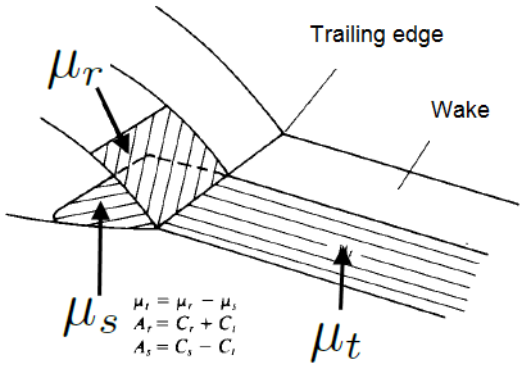

Figure 2: Relation between trailing edge panel and trailing edge panels [3]

Thus, the Eq. 10 can be rewrite in a simlpe form:

$$\sum_{k=1}^{N} A_k \mu_k = -\sum_{k=1}^{N} B_k \sigma_k, \tag{15}$$

where, $A_k = C_k$ if k don't belong a trailing edge panel and, $A_k = C_k \pm C_t$ if k belong a trailing edge panel.

The application of boundary condition, Eq. 15, for each control point will result in an system of linear equation,

$$\begin{pmatrix} a_{11} & a_{12} & \cdots & a_{1N} \\ a_{21} & a_{22} & \cdots & a_{2N} \\ \cdots & \cdots & \cdots & \cdots \\ a_{N1} & a_{N2} & \cdots & a_{NN} \end{pmatrix} \begin{pmatrix} \mu_1 \\ \mu_2 \\ \vdots \\ \mu_N \end{pmatrix} = \begin{pmatrix} RHS_1 \\ RHS_2 \\ \vdots \\ RHS_N \end{pmatrix}, \tag{16}$$

with,

$$\begin{pmatrix} RHS_1 \\ RHS_2 \\ \vdots \\ RHS_N \end{pmatrix} = - \begin{pmatrix} b_{11} & b_{12} & \cdots & b_{1N} \\ b_{21} & b_{22} & \cdots & b_{2N} \\ \cdots & \cdots & \cdots & \cdots \\ b_{N1} & b_{N2} & \cdots & b_{NN} \end{pmatrix} \begin{pmatrix} \sigma_1 \\ \sigma_2 \\ \vdots \\ \sigma_N \end{pmatrix}. \tag{17}$$

The a_{ij} e b_{ij} are known by influence coefficient matrices.

2.4 Calculation of Pressures and Loads

The tangencial local velocity on each control point can be calculated by differentiating the velocity potential along the tagential direction (l, m),

$$q_l = \frac{\partial \mu}{\partial l}, \tag{18}$$

$$q_m = \frac{\partial \mu}{\partial m}, \tag{19}$$

and for the normal direction,

$$q_n = -\sigma. \tag{20}$$

The total velocity on panel k is the sum of local velocity with the velocity of free-stream

$$\mathbf{Q}_k = (Q_{\infty_l}, Q_{\infty_m}, Q_{\infty_n})_k + (q_l, q_m, q_n)_k. \tag{21}$$

The pressure coeficient can be computed by,

$$Cp_k = 1 - \frac{Q_k^2}{Q_\infty^2} \tag{22}$$

The contribution of each panel for the aeodynamic force is,

$$\mathbf{\Delta F_k} = Cp_k \left(\frac{1}{2} \rho Q_\infty^2 \right) \Delta S_k \mathbf{n_k}. \tag{23}$$

where ρ is the density of fluid and ΔS_k area of panel k.

The total force on body immersed on inviscid flow is calculated with the sum of increments $\mathbf{\Delta F_k}$ of each panel. This force can be decomposed in perpendicular and parallel direction of the free-stream. The first one is the lift force and the second induced drag force.

Lift and induced drag coefficient are :

$$C_L = \frac{L}{(0.5\rho Q_\infty^2)S}, \tag{24}$$

$$C_D = \frac{D_{ind}}{(0.5\rho Q_\infty^2)S} \tag{25}$$

where S is the reference area

3 Ground Effect

A body sustainer operating close to the ground exhibit a change in the aerodynamics characteristics when compared with a case where the ground isn't present. The aerodynamic characteristics are changed due to two phenomena: the ground effect and the Ventury effect. While in the first there is an increased lift and decreased drag, in the second the lift decrease and the drag increases significantly[5, 6].

Since the construction of the computucional tool, in this work, is made using the panel method, the simulation of the effect of a solid surface by the body passes trough using the method of images.

3.1 Atmospheric Boundary Layer

One way to approach the velocity profile of the atmospheric boundary layer involves the use of a logarithmic function [7]:

$$u(z) = u(z_r) \frac{ln(\frac{z}{z_0})}{ln(\frac{z_r}{z_0})}, \tag{26}$$

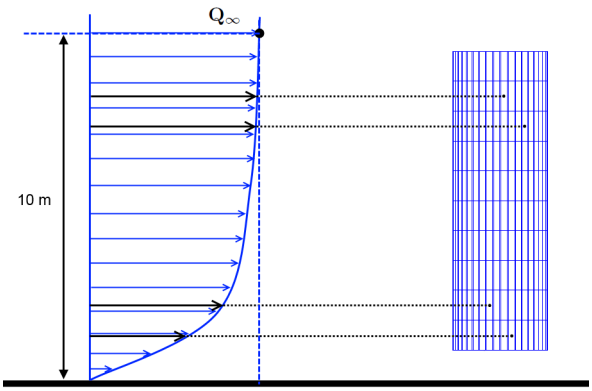

Figure 3: Atmospheric boundary layer

where z_r is a reference height, $u(z_r)$ the reference velocity, z_0 surface rughness and z is the height above the mean water surface. The surface rughness z_0 varies with sea conditions: 0,2 for calm sea and 0,5 for blown sea. The reference height z_r for a reference velocity $u(z_r)$ is typically 10 meters[7].

For each panel k, is calculated the height z that it is from the ground and the velocity $u(z)$corresponding to this height in the atmospheric boundary layer, Eq. 26, with a reference velocity $u(z_r)$ equal to the free stream velocity Q_∞. The panels closest to the ground will be subject to a lower velocity than those who are felt in higher heights. Thus, the aerodynamic characteristics of the wing inside the atmospheric boundary layer are changed since the solution of Eq. 16 takes into account the variation of free stream velocity (Eq. 17). Fig. 3 represents, in schematic form, what was described above.

4 Coupled Viscous Effects

The viscous effects can be add to the inviscid solution through a simulation of displacement tickness with a transpiration velocity:

$$V_w = \frac{d}{dx}\left(U_e \delta^*\right) \tag{27}$$

4.1 Interaction with XFOIL

The XFOIL is used in this work to calculate the boundary layer parameter δ^*, important for the purposes of coupling the viscous solution to inviscid solution trough Eq. 27.

Since the XFOIL is a tool of analysis of bidimensional airfoils and this study is about a tridimensional flow, it was assumed that the boundary layer developed on the body surface can be approximated by several bidimensional boundary layers along the wingspan[8, 9, 10, 11, 12]. The wing is split into bidemension sections wich will subsequently be analyzed independently by XFOIL.

4.1.1 Wing

For a single wing, the data necessary for an viscous analysis by the XFOIL, for each section, are the following:

- Airfoil
- Reynolds number
- Effective angle of attack (α_{ef})

After the analysis of a specific section, one of the outputs of XFOIL - parameter δ^*- is used for calculate the transpiration velocity Eq. 27.

Another parameter of the boundary layer that is obtained by the analysis of each section of the wing is the drag coefficient due to shear stress on the body surface $C_{D\tau_w}$. This parameter is used to calculate the total drag.

4.1.2 Flap

Regarding the analysis on the flap, and taking into account the difficulty in predicting the effective angle of attack that particular section of this element is subject, the input to XFOIL is as follows:

- Airfoil
- Reynolds Number
- Section Lift Coefficient (C_l)

Note that both the effective angle α_{ef} and the lift coefficient of the flap C_l section are obtained from the inviscid flow solution so that, all the iterative process, for the calculation of the parameters of the boundary layer, is performed by XFOIL.

Repare-se que tanto o ângulo efectivo α_{ef} como o coeficiente de sustentação da secção do flap C_l são obtidos a partir da solução do escoamento invíscido pelo que todo o processo iterativo, para o cálculo dos parâmetros da camada limite, fica a cargo do XFOIL.

The next chapter will seek to explain the way in which the displacement thicknesses, obtained for each section, are coupled to inviscid model through a velocity transpiration on the body surface.

4.2 Numerical Procedure

A precise way to represent the total flow, which takes into account the influence of the boundary layer and the inviscid solution, is accomplished with an additional term in the intensities of the sources[13, 8, 9].

$$\sigma = \sigma^{inv} + \sigma^{vis} \tag{28}$$

where σ^{vis} is the new term of the source to add the displacement thickness. Note that this term is added to the body surface and wake.

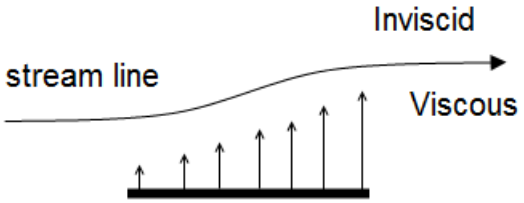

Figure 4: Stream line displacement by transpiration velocity

The solution of the total flow can be considered a result of the addition between the inviscid e viscous solutions,

$$\mu = \mu_{inv} + \mu_{vis}. \tag{29}$$

where the term μ_{inv} is calculated by the Eq. 16. The Eq. 29 only depends on the term σ^{vis} and can be written in this way:

$$\mu = \mu_{inv} + H\sigma^{vis} \tag{30}$$

with,

$$H = a^{-1}(-b^{vis}) \tag{31}$$

where a and b are the matrices of influence coefficients with dimensions $(N \times N)$ e $(N \times (N + N_w))$.

The only unknown in Eq. 30 is the column vector σ^{vis}. This vector contains the intensities of each panel required for the displacement of the stream lines, in order to simulate the displacement thickness (Fig. 4).

5 Results

5.1 Ground Effect

The data and the results of the problem can be consulted in [5].

For the simulation with 3D panel method, several angles of attack were analyzed for different distances from de trailing edge to ground h. In Fig. 5 is presented an overlay of the results obtained with panel method and with STAR-CCM+ where the lift coefficient as in function of h/c.

The major difference, regarding to the results of the lift coefficient obtained with both methods, occurs when the wing is close to the ground at a low angle of attack. This is due to the fact that the solution of panel method, contrary do the solution of STAR-CCM+, don't take into acount the viscosity. Thus, the velocities developed between the soil and the lower wing surface are quite high, which leads

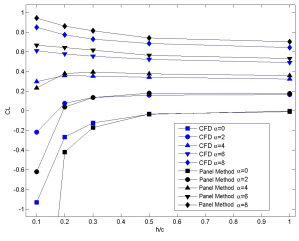

Figure 5: Comparison of results obtained by the results of the panel method with STAR-CCM+

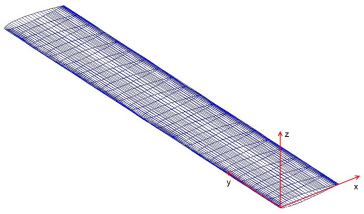

Figure 6: Grid on rectangular wing

to a very negative lift coefficient (down force), as shown in Fig. 5 (for an angle attack equal to 0°)

Note that for this wing with a symmetrical airfoil NACA0015, the occurrence of the ground effect and the Ventury effect depends from the angle attack. For angles of attack below 4° , the Ventury effect is dominant; for angles attack over 4° , the lift coefficient increases as the wing decreases height from the ground, with the ground effect being the dominant.

Thus, the method of images, incorporated into the 3D panel method, is able to simulate with accuracy the changes in the aerodynamic characteristics of a wing due to the presence of a solid surface.

5.2 Rectangular Wing

A comparison was made between the experimental and numerical results for a rectangular wing with 6m wingspan, 1 m chord and with a NACA 0012 airfoil. The experimental activity is described in [14]. The grid used, from where the numerical solution was obtained by the 3D panel method, has 60 panels in the direction of the chord and 20 in the direction of the wingspan, as shown in Fig. 6.

At the comparison of the numerical results - that takes into account the viscous effects - with experimental results, it was considered a Reynolds number equal to 1.92×10^6 of the experimental procedure.

To the angle of maximum lift, 18° , the results have a maximum relative error of 2%; after this angle, the difference in results is evident.

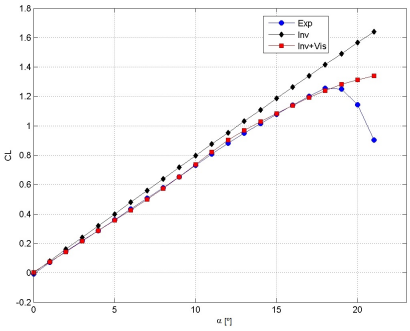

Figure 7: CL vs alpha for a rectangular wing at a Reynolds equal to 1.92×10^6

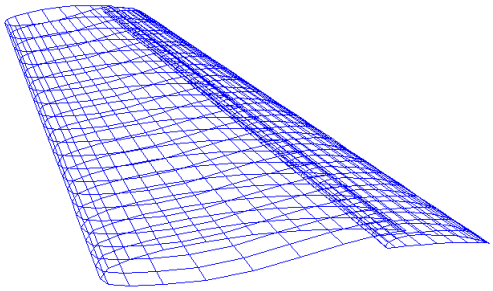

Figure 8: Wing-Flap configuration

5.3 Wing with Flap

The RAE wing tested in [15], is constructed with a airfoil with a maximum thickness of 11.7 % occuring at 37.5% chord and the maximum camber occurring at 75% chord. The experimental activity was done at a Reynolds of 1.35×10^6.

The experimental results, which will consititue henceforth the reference results to be compared with the computational ones, were obtained for two different experimental situations: a flap with angle 10° and 25°.

Given the simetry of the wing geometry, only one half of the wing was simulated. The other half was simulated by means of the method of image, i.e., it was used the same method as the one deveopled in the section *Ground Effect*, with a heigth to the ground $h = 0$. The mesh used in the wing ans flap was constitued by 100 panels in the direction of the chord (50 upper surface + 50 lower surface) and 20 panels in the span direction.

The simulation results of a inviscid flow around a wing-flap aggregate were satisfactory if one takes into account the complexity of the analysed geometry. For angles of attack up to approximately 8° the relative error showed to be in the majority higher than 10% and lower than 13.6%. When the wing begins to lose lift, the inviscid case results, linear

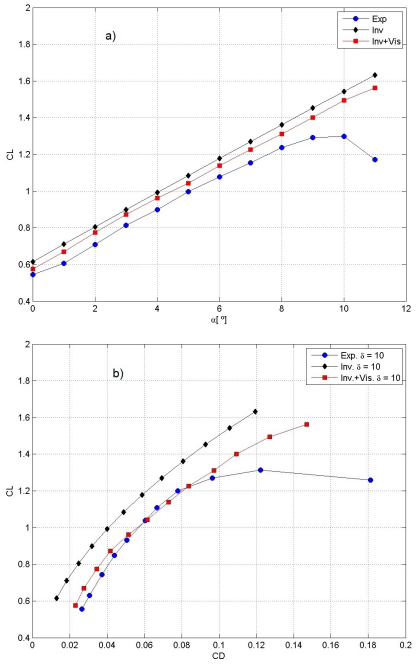

Figure 9: Lift and drag coefficients for a deflection angle of 10° para o flap. a) CL vs α, b) CL vs CD

within the studied range, begins to deviate, presenting relative erros of 18.8% and 39.2% for angles attack of 10° and 11°, respectively.

In the simulation where the viscous effects were taken into account, the relative erros were always lower than 9.3% for angles attack up to 8°. In summary, the introduction of viscous effects in the simulation allowed a curve CL vs α prediction with higher accuracy.

Fig. 9 b) ilustrates the curve CL vs CD for the experimental results, inviscids and with the coupling of the viscous effects. It is shown the improvement introducted in the prediction of this curve after the introduction of the viscous effects into the inviscid solution.

In average, the relative error for a flow with an attack angle within the range of attack angles that follow a linear evolution regarding the experimental lift coefficients, inviscid and viscous are 11.2% and 6.7%, respectively.

6 Conclusions

The three-dimensional (3-D) simulation of the aerodynamic behaviour of an inviscid, incompressible and irrotational flow around a sustainer body was achieved by means of the 3-D panels method, implemented computationaly in the MATLAB environment. Such approach revealed to be fast in the calculus of the final solution and accurate when compared with experimental results.

To the 3-D panels method it was introduced the method of image, an option that allowed the simulation of flows around sustainers bodies operating near the ground. This methodology demonstrated capability in predicting two characteristics phenomenons of such flows: the ground effect and Venturi. Regarding the former, it was showed that the variation of the aerodynamics characteristics were predicted with good accuracy. However, this was not the case of the latter, the predicted intensity of lift and drag coefficients showed to differ considerably when compared with experimental ones. This discrepancy related with the fact that the panels methods do not consider the viscous effects. Neverthless, the computational obtained patterns regarding the aerodynamic behavior of the aforementioned coefficients showed to be quiet satisfactory.

The panels method formulation was slightly altered in order to account the velocity change inside an atmospheric boundary layer. This was done by adopting a velocity change model following a ln analytical function.

To the inviscid flow was coupled the viscous effects by using a transpiration velocity, applied on the body surface. This was done to simulate the displacement of the stream lines. The transpiration velocity was calculated through the variation of the displacement thickness along the wing. The boundary layer developed on the surface of the sustainer body was considered bidimensional and therefore the wing was divided in several cross section, each of them treated separately. The analyse of each one was done using the XFOIL program. The application of this coupling showed to improve considerably the results, mainly in the prediction of the Drag coefficients, as the relative errors between them and the experimental ones decreased sharply.

It was concluded that the developed code may constitute a valuable computational tool in a preliminary design stage of lifting surfaces.

7 Appendix

The velocity potential for a flat panel with a constant source strength [3]:

$$\Phi_f = \frac{-\sigma}{4\pi}\{[aux1_{12} + aux1_{23} + aux1_{34} + aux1_{41}] + \\ + \mid z \mid [aux2_{12} + aux2_{23} + aux2_{34} + aux2_{41}]\} \tag{32}$$

and, for a flat panel with constant doublet strength:

$$\Phi_d = \frac{\mu}{4\pi}\left[aux2_{12} + aux2_{23} + aux2_{34} + aux2_{41}\right] \tag{33}$$

with,

$$aux1_{ij} = \frac{(x - x_i)(y_j - y_i) - (y - y_i)(x_j - x_i)}{d_{ij}} \times \\ \times \ln\left(\frac{r_i + r_j + d_{ij}}{r_i + r_j - d_{ij}}\right), \tag{34}$$

$$aux2_{ij} = \arctan\left(\frac{m_{ij}e_i - h_i}{zr_i}\right) - \tag{35}$$

$$- \arctan\left(\frac{m_{ij}e_j - h_j}{zr_j}\right), \tag{36}$$

where,

$$d_{ij} = \sqrt{(x_j - x_i)^2 + (y_j - y_i)^2}, \tag{37}$$

$$m_{ij} = \frac{y_j - y_i}{x_j - x_i}, \tag{38}$$

and,

$$r_k = \sqrt{(x - x_k)^2 + (y - y_k)^2 + z^2}, \tag{39}$$

$$e_k = (x - x_k)^2 + z^2, \tag{40}$$

$$h_k = (x - x_k)(y - y_k), \tag{41}$$

for k = 1, 2, 3 e 4.

References

[1] http://www.optimal.pt/Site/Home.html (05/12/2013).

[2] http://www.tonycastro.co.uk/ (05/12/2013).

[3] Joseph Katz and Allen Plotkin. *Low-Speed Aerodynamic: from wing theory to panel methods*. McGraw-Hill, 1991.

[4] Vasco de Brederode. *Fundamentos de Aerodinâmica Incompressível*. Vasco de Brederode, 1997.

[5] Juhee Lee. Aerodynamic characteristics of rectangular wing with square laternal tip. In *51st AIAA Aerospace Sciences Meeting Iincluding The New Horizons Forum And Aerospace Exposition*, 2013.

[6] Th. Lutz S. Schmid and E. Kramer. Impact of modelling approaches on the prediction of ground effect aerodynamics. 3:419–429, 2009.

[7] Nils Haack. C-class catamaran wing performance optimisation. Master's thesis, University of Manchester, 2011.

[8] Gary S. Hufford. Viscous flow around marine propeller using boundary layer strip theory. Master's thesis, Massachusetts Institute Of Technology, 1992.

[9] Xiangming Yu. Three dimensional viscous/inviscid interactive method and its application to propeller blades. Master's thesis, The University of Texas at Austin, 2012.

[10] Anders Karlsson Kamran Mohseni Salvatore Lupo, Henrik Nyberg. Xwing - a 3d viscous design tool for wings. In *46th AIAA Aerospace Sciences Meeting and Exhibit*, 2008.

[11] Dale L. Ashby. Potential flow theory and operation guide for the panel code pmarc. Technical report, NASA, 1999.

[12] Brian Maskew. Program vsaero theory document - a computer program for calculating nonlinear aerodynamic characteristics of arbitrary configuration. Technical report, NASA, 1987.

[13] William Michael Milewski. Three-dimensional viscous flow computations using the integral boundary layer equations simultaneously coupled with a low order panel method. Master's thesis, Massachusetts institute of technology, 1997.

[14] Long P. Yip and Gary L. Shubert. Pressure distributions on a 1 by 3 meter semispan wing at sweep angles from 0 to 40 in subsonic flow. Technical report, NASA, 1976.

[15] D. A. Lovell. A wind-tunnel investigation of the effects of flap span and deflection angle, wing planform and body on the high-lift performance of a 28^o swept wing. Technical report, R.A.E. CP 1372, 1977.